Local scale-invariance of the 2+1 dimensional Kardar–Parisi–Zhang model

2017 J. Phys. A: Math. Theor. 50 12LT01

(http://iopscience.iop.org/1751-8121/50/12/12LT01)

Letters

IOP Publishing Journal of Physics A: Mathematical and Theoretical

J. Phys. A: Math. Theor. **50** (2017) 12LT01 (9pp) doi:10.1088/1751-8121/aa5d87

Letter

Local scale-invariance of the 2 + 1 dimensional Kardar–Parisi–Zhang model

Jeffrey Kelling[2,3], Géza Ódor[1] and Sibylle Gemming[3,4]

[1] Institute of Technical Physics and Materials Science, Centre for Energy Research of the Hungarian Academy of Sciences, PO Box 49, H-1525 Budapest, Hungary
[2] Department of Information Services and Computing, Helmholtz-Zentrum Dresden-Rossendorf, PO Box 51 01 19, 01314 Dresden, Germany
[3] Institute of Ion Beam Physics and Materials Research, Helmholtz-Zentrum Dresden-Rossendorf, PO Box 51 01 19, 01314 Dresden, Germany
[4] Institute of Physics, TU Chemnitz, 09107 Chemnitz, Germany

E-mail: odor@mfa.kfki.hu

Received 4 October 2016, revised 12 January 2017
Accepted for publication 1 February 2017
Published 20 February 2017

Abstract

Local scale-invariance theory is tested by extensive dynamical simulations of the driven dimer lattice gas model, describing the surface growth of the 2 + 1 dimensional Kardar–Parisi–Zhang surfaces. Very precise measurements of the universal autoresponse function enabled us to perform nonlinear fitting with the scaling forms, suggested by local scale-invariance (LSI). While the simple LSI ansatz does not seem to work, forms based on logarithmic extension of LSI provide satisfactory description of the full (measured) time evolution of the autoresponse function.

Keywords: local scale-invariance, Kardar–Parisi–Zhang, GPGPU, autoresonse

(Some figures may appear in colour only in the online journal)

Understanding universal scaling behavior of nonequilibrium dynamical systems is a challenging task [1]. Critical phenomena can emerge away from equilibrium, but due to the broken time reversal and translational symmetries, an extension of the renormalization group method (RG), as the best tool, is not straightforward [2]. The lack of translational symmetry manifests in aging phenomena observed in glasses, polymers, reaction-diffusion systems or cross-linked networks [3].

LSI theory is proposed [4] to generalize dynamical scaling to a larger set of local scale transformations, including $t \to t/(1 + t\gamma)$, analogously as conformal invariance (CI) extends RG of equilibrium critical phenomena. As CI [5, 6] works well in case of equilibrium universality classes, LSI aims at the same for nonequilibrium dynamical ones [7]. LSI has been

shown to reproduce the universal shapes of responses and correlators in a large variety of models, as reviewed in detail in [7]. The predictive power of generalized dynamical scaling alone was shown to be limited [8], and later the role of the generalized Galilei invariance was recognized. Analogously to the logarithmic CI generalization [9], Henkel suggested the logarithmic extension of LSI (LLSI) to make the theory applicable for more general cases [10].

While many systems are described by a single dynamical length scale $L(t) \sim t^{1/z}$, with the dynamical exponent z [11, 12], aging ones are best characterized by two-time quantities, such as the dynamical correlation and response functions [13]. In the aging regime: $s \gg \tau_{\rm m}$ and $t - s \gg \tau_{\rm m}$, where $\tau_{\rm m}$ is a microscopic time scale, one expects the following law for the autoresponse function of the field ϕ:

$$R(t,s) = \left.\frac{\delta\langle\phi(t)\rangle}{\delta j(s)}\right|_{j=0} = s^{-1-a} f_R\left(\frac{t}{s}\right) \tag{1}$$

where s denotes the start and $t > s$ the observation time, j is the external conjugate to ϕ. This law contains the so-called aging exponent a, the universal scaling function, with the asymptotic behavior $f_R(t/s) \sim (t/s)^{-\lambda_R/z}$, and the autoresponse exponent λ_R.

LSI has been shown to describe aging properties of diffusive, solvable models with $z = 2$, like Acetri [14, 15], Edwards–Wilkinson (EW) [16] interface growth and of mean-field like models, exhibiting long-range interactions [7, 17]. It also provided agreement with the numerics in case of reaction-diffusion models [18–20]. However, tests in the critical $(1 + 1)$-dimensional contact process showed systematic deviations in the $t/s \to 1$ limit [10, 21]. On a phenomenological level, these discrepancies could be resolved by the more recent extension to LLSI [10], which we shall recall below.

Numerical testing is easier in systems, which do not need to be tuned to criticality, but exhibit generic scale invariance, like interface models. For nonequilibrium surface growth dynamics the LLSI predictions have been found to be in agreement with the simulations of the $1 + 1$ dimensional Kardar–Parisi–Zhang (KPZ) model [22]. The purpose of the present study is to extend such investigation to $2 + 1$ dimensions in the presence of high precision simulation data available by simulations of dimer models describing KPZ surface growth [23–25].

The KPZ equation [26] describes the evolution of the height function $h(\mathbf{x}, t)$ in the d dimensional space relative to its mean position

$$\partial_t h(\mathbf{x},t) = \nu\nabla^2 h(\mathbf{x},t) + \lambda(\nabla h(\mathbf{x},t))^2 + \eta(\mathbf{x},t), \tag{2}$$

where λ is the amplitude of the up-down anisotropy, ν is a smoothing surface tension coefficient and η is a roughening of the surface and represents Gaussian noise with zero mean value and the variance $\langle\eta(\mathbf{x},t)\eta(\mathbf{x}',t')\rangle = 2T\nu\delta^d(\mathbf{x}-\mathbf{x}')(t-t')$. The letter T is related to the noise amplitude (the temperature in the equilibrium system).

This equation was inspired in part by the stochastic Burgers equation [27] and can describe the dynamics of simple growth processes in the thermodynamic limit [28], randomly stirred fluids [29], directed polymers in random media [30], dissipative transport [31, 32], and the magnetic flux lines in superconductors [33].

The morphology of the surface is usually characterized by the roughness

$$W(L,t) = \sqrt{\langle h^2(\mathbf{x},\mathbf{t})\rangle_{\mathbf{x}} - \langle h(\mathbf{x},\mathbf{t})\rangle_{\mathbf{x}}^2}, \tag{3}$$

where $\langle\ \rangle_{\mathbf{x}}$ denotes an average over all spatial coordinates. Simple growth processes are expected to be scale invariant and follow the Family–Vicsek scaling law [34]:

$$W(L,t) \sim L^{\alpha} f(t/L^z), \tag{4}$$

with the universal scaling function $f(u)$

$$f(u) \sim \begin{cases} u^{\beta} & \text{for } u \ll 1 \\ \text{const.} & \text{for } u \gg 1. \end{cases} \tag{5}$$

Here, α is the roughness exponent, describing the stationary state, where the correlation length exceeds the lateral system size L. The growth regime is governed by the growth exponent β. The ratio of these gives the dynamical exponent $z = \alpha/\beta$. KPZ is Galilei invariant [29], resulting in the exponent relation

$$z = 2/(1 + \beta). \tag{6}$$

Discrete models set up for KPZ have been studied a lot in the past decades [35–37]. A mapping between KPZ surface growth in two dimensions and driven lattice gases has been advanced in [23]. This is based on the so-called octahedron model, characterized by binary slope variables at the middle points of the up/down edges. Up slopes in the x or y directions are represented by $\sigma_{x/y} = 1$, while down ones are encoded by $\sigma_{x/y} = 0$. Thus deposition or removal of octahedra corresponds to a stochastic cellular automaton with the simple update rules

$$\begin{pmatrix} 0 & 1 \\ 0 & 1 \end{pmatrix} \underset{q}{\overset{p}{\rightleftharpoons}} \begin{pmatrix} 1 & 0 \\ 1 & 0 \end{pmatrix} \tag{7}$$

with probability p (q) for attachment (detachment). By considering edge values to be lattice occupancy variables we can map the octahedron model onto self-reconstructing dimers following an oriented migration in the bisection of x and y directions (see figure in [23]). The surface height can be reconstructed for each lattice site from the slope variables by tracing a path from a reference point: (1, 1) with $h_{1,1} := 0$, leading to the expression

$$h_{i,j} = \sum_{l=1}^{i} [2\sigma_x(l, 1) - 1] + \sum_{k=1}^{j} [2\sigma_y(i, k) - 1]. \tag{8}$$

We have confirmed that this mapping using the parameterization: $\lambda = 2p/(p + q) - 1$ reproduces the one-point functions of the continuum model [23]. The case $p \approx q$, leading to $\lambda \approx 0$, the EW model is recovered. Numerical results for the autocorrelation have also been found to be in agreement with those of other KPZ models [25, 38, 39]. The dimer lattice gas can be studied by very efficient bit coded simulation methods using graphic cards (GPU) as detailed in [25, 40].

We performed extensive simulations of the dimer model on lattices with lateral size of $L = 2^{16}$ and periodic boundary conditions. The large systems serve to stay clear of finite size effects. The initial state corresponded to the flat surface and rule (7) was applied either by a random-sequential (RS) [25] or a sub-lattice parallel stochastic cellular automaton (SCA) site selection algorithm.

We calculated the autoresponse function as described in [25]. To introduce a perturbation, we used space-dependent attachment and detachment probabilities

$$p_i = \begin{cases} p_0 + a_i\varepsilon/2 & \text{if } p_0 + a_i\varepsilon/2 \in [0, 1] \\ 1 - \varepsilon/2 + a_i\varepsilon/2 & \text{otherwise} \end{cases} \tag{9}$$

and $q_i = p_0 + q_0 - p_i$, respectively. Here, $a_i = \pm 1$ and $\varepsilon = 0.005$ is a small parameter. After the waiting time s we used the same stochastic noise η (random sequences), in two realizations. System A evolved, up to the waiting time s, with the site-dependent probabilities p_i and q_i and afterwards with the uniform ones p_0 and $q_0 = 0$. System B evolved always with spatially uniform attachment and detachment.

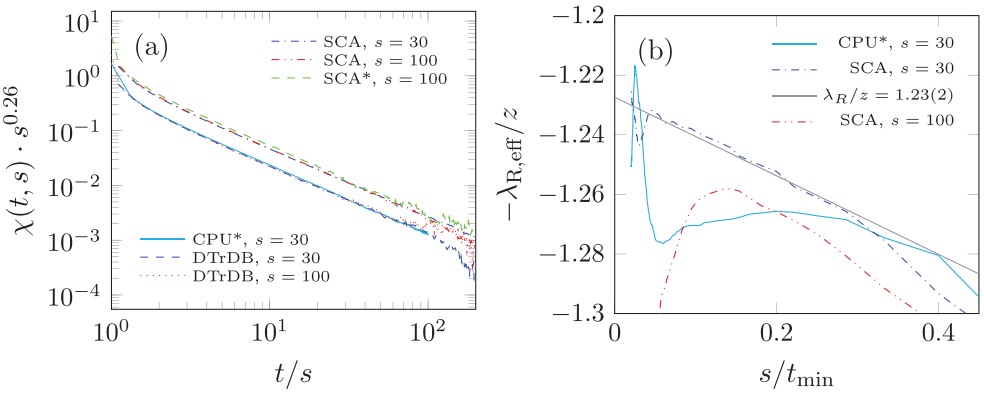

Figure 1. Simulation results of the integrated height autoresponse, comparing variants obtained by RS and SCA simulations. (a) Aging collapse of the functions. (b) Corresponding effective exponents, extrapolating to asymptotic values. Slopes of DTrDB and SCA* are not shown, because the late-time regime was too noisy, due to small sample sizes. The black straight line corresponds to a linear fit to the SCA $s = 30$ results. System and sample sizes are: $L_{\mathrm{CPU}*} = 2^{13}$, $n_{\mathrm{CPU}*} = 39083$ [25], all others use $L = 2^{16}$, with $n_{\mathrm{SCA},s=30} = 23849$, $n_{\mathrm{SCA},s=100} = 12012$, $n_{\mathrm{SCA}*,s=100} = 1390$, $n_{\mathrm{DTrDB},s=30} = 830$ and $n_{\mathrm{DTrDB},s=100} = 700$.

From these simulations, we determined the time-integrated response function

$$\chi(t,s) = \int_0^s \mathrm{D}u\, R(t,u) = \frac{1}{L^2}\sum_{\vec{r}}^{L^2}\left\langle \frac{h_{\vec{r}}^{(A)}(t,s) - h_{\vec{r}}^{(B)}(t)}{\varepsilon\Delta}\right\rangle = s^{-a} f_\chi\left(\frac{t}{s}\right), \tag{10}$$

where a is the aging exponent for the autoresponse. Measurements were performed at exponentially increasing times

$$t_{i+1} = (t_i + 10)\cdot \mathrm{e}^m, \quad \text{with} \quad m > 0, \quad t_0 = 0,$$

up to $t_{\mathrm{max}} = 200 \cdot s$. Throughout this paper time is measured in Monte-Carlo steps MCS), defined as one sweep over all lattice sites.

The random-sequential GPU implementation from [25] has been modified using a novel combination of the dead border and double tiling domain-decomposition schemes, which we call DTrDB, in order to eliminate previously observed correlations. Details of this algorithm will be discussed elsewhere [41]. To speed up simulations further, we introduced a SCA algorithm on GPUs, which uses a checkerboard pattern for updates: a MCS is performed by updating all odd sites simultaneously with $p < 1$ and all even sites afterwards [42]. The GPU implementations were tested by comparing different schemes. Direct comparison of the GPU results with sequential CPU simulations was impossible on the same level of accuracy, but consistency with former simulations [25] could be achieved.

Results from various autoresponse calculations are summarized in figure 1(a). The forms of the autoresponse function agree very well across all types of simulations. The most notable difference is a constant factor ($\sim$2.08) in the response functions between the SCA and RS results, which is caused by model-dependent time-scales. Also note the small shift between SCA ($p = 0.95\, q = 0$) and SCA* ($p = 0.95, q = 0.05$) for $s = 100$, caused by the different update probabilities.

Table 1. Estimates for the height autoresponse exponent λ_R, assuming $z = 1.611(2)$. Sample and system sizes are listed below figure 1. Error-margins were estimated visually.

	CPU∗ [25] $p = 0.98, q = 0.02$	SCA $p = 0.95, q = 0$
λ_R/z	1.25(3)	1.23(2)
λ_R	2.01(5)	1.98(4)

The aging exponent is often determined by performing a manual collapse of the available datasets for different waiting times s. For RS simulations, the value $a_{\mathrm{RS}}^{\mathrm{coll.}} = 0.30(1)$ was determined in this way and published in [25]. For the SCA simulations presented in figure 1(a), the value $a_{\mathrm{SCA}}^{\mathrm{coll.}} = 0.26(1)$ shows the best collapse. However, this method requires visual inspection of plots to determine for which value of $a^{\mathrm{coll.}}$ the data collapse works best, which is prone to bias and underestimation of the attached error margins.

Numerical computation of the aging exponent involves point-wise division of autocorrelation functions for different waiting times:

$$\frac{\chi(t,s_1)}{\chi(t,s_2)} = \frac{s_1^a f_\chi(t/s_1)}{s_2^a f_\chi(t/s_2)} \overset{(t/s_1 = t/s_2)}{=} \left(\frac{s_1}{s_2}\right)^a.$$

Since the values $\langle\chi(t,s)\rangle$ are available only at discrete times an interpolation is required to compute these ratios at arbitrary t/s. The simplest option is a linear one, which can also be performed on a double-logarithmic scale, reducing systematic errors when the interpolation values follow a power law. In the implicit average over t all points are weighted with their statistical signal-to-noise ratio, which overall increases the weight of early times, while in the visual method one is tempted to focus on late times. The present method yields $a_{\mathrm{SCA}} = 0.24(2)$, for the SCA simulations with $q = 0$, and $a_{\mathrm{DTrDB}} = 0.27(2)$, for our new RS simulations with $p = 1$, $q = 0$. For comparison, we calculated $a_{\mathrm{RS}} = 0.25(4)$ from the data published in [25], based on RS CPU and GPU simulations. The present data suggest no significant difference between the aging exponents of RS and SCA.

In order to determine the asymptotic scaling and corrections we determined (tail) effective exponents $\lambda_{R,\mathrm{eff}}(t_{\mathrm{min}})/z$, where each value is the exponent of a power-law fit to $\chi(t,s)$ in the interval $(t_{\mathrm{min}}, t_{\mathrm{max}})$ using the form

$$g_{t_{\mathrm{min}}}(t) = c \cdot t^{-\lambda_{R,\mathrm{eff}}(t_{\mathrm{min}})/z}, \tag{11}$$

with free parameters c and $\lambda_{R,\mathrm{eff}}(t_{\mathrm{min}})/z$. The results are displayed in figure 1(b) for the three largest datasets, where $t_{\mathrm{min}} \lesssim t_{\mathrm{max}}/4$. This method suppresses short-wavelength noise but preserves scaling corrections of larger scales. Only our best dataset (SCA, $s = 30$) allows a reliable extrapolation for $\lambda_{R,\mathrm{eff}}(t_{\mathrm{min}} \to \infty,)/z$. The effective exponent curve of the $s = 100$ data breaks down at the end; still the trend observed at early times is in agreement with the extrapolations for $s = 30$. We attribute this to larger oscillations, similarly as in the case of CPU RS updates, where, however, the asymptotic value still appears to agree.

Table 1 summarizes the estimates for the autoresponse exponent λ_R. Here we assume $z = 1.611(2)$, that can be obtained by the scaling relation (6) and using our former, high precision value $\beta = 0.2415(15)$ [24]. There is agreement between the results for the considered waiting times across RS and SCA dynamics.

Considering, that earlier results for the autocorrelation exponent marginally allow $\lambda_C = 2$ [25], which is predicted by Krug's conjecture $\lambda_C = d$ [43, 44], it is interesting to note, that $\lambda_R = 2$ seems to be satisfied within error margin. The possible equality $\lambda_C = \lambda_R$ might point to the existence of a non-equilibrium fluctuation-dissipation relation in $(2+1)$-dimensional KPZ. The autocorrelation function is defined as

$$C(t,s) = \langle \phi(t)\phi(s)\rangle - \langle \phi(t)\rangle\langle \phi(s)\rangle \sim s^{-b}(t/s)^{-\lambda_C/z},$$

with the aging exponent $b = -2\beta$ and definitions analogous to those in equation (1). However, one must expect a different relation than in the $(1+1)$-dimensional case, because the implied relation for the aging exponents $1 + a = b + 2/z$ [22] does not hold.

The quality of the available data allows a precise calculation of effective exponents. Yet, the estimates for the asymptotic values carry larger uncertainties, due to the unknown corrections to scaling. Thus, a next step in the KPZ aging studies is an attempt to determine these corrections, assuming scaling forms for χ_R. These forms are based on the LSI hypothesis. For the time-integrated autoresponse, equation (10), LSI theory for KPZ predicts the scaling function

$$f_{\chi,\mathrm{LSI}}(t/s) = A_0(t/s)^{-\lambda_R/z}(1 - s/t)^{-1-a'}, \tag{12}$$

where A_0 is a normalization factor and a' is expected to be another universal exponent, like the aging exponent a. A different form, adding logarithmic corrections was proposed recently in [10]:

$$\begin{aligned} f_{\chi,\mathrm{L^2LSI}} = (t/s)^{1-\lambda_R/z}\,[&A_0(1-(1-s/t)^{-a'}) \\ &+ (1-s/t)^{-a'}\cdot(A_1\ln(1-s/t) + A_2\ln^2(1-s/t))]\,, \end{aligned} \tag{13}$$

where the sum of logarithmic terms to second order results from the assumption, that the primary field ϕ of the system is replaced by a doublet and the scaling dimensions are represented by 2×2 matrices. The solution in [10] uses a Schrödinger-invariant Lie algebra, which implies $z = 2$, a dynamical exponent different from that of the KPZ universality class. However, the scaling form (1) is invariant of the value of z, because it depends on the ratio λ_R/z only. It should be noted, that, this does not hold for the space-dependent part of the response function, which remains an open problem.

The scaling function (13) resembles a form, which contains the first two lowest order correction terms of a logarithmic series to (12). We shall test by fitting if, an assumed more generalized power series form

$$\begin{aligned} f_{\chi,\mathrm{L^JLSI}} = (t/s)^{1-\lambda_R/z}\Bigg[&A_0(1-(1-s/t)^{-a'}) \\ &+ (1-s/t)^{-a'}\cdot\sum_{j>0}^{J} A_j\ln^j(1-s/t)\Bigg], \end{aligned} \tag{14}$$

which, given enough terms, might fit a broad range of data, really supports the expected $\mathrm{L^2LSI}$ theory with the scaling (13). However, an LSI extension with triplets, or beyond, would also give physical meaning to some terms with $j \geqslant 3$. Thus these terms being relevant to describe the data would point to the necessity of higher orders in the extension of LSI.

We have tested different (J) levels of the series (14) with our data, obtained from the most precise SCA simulations. Figure 2 shows plots of the ratio of data and best fit. This is a visual representation of how well forms for $J \in [0,3]$ describe the data:

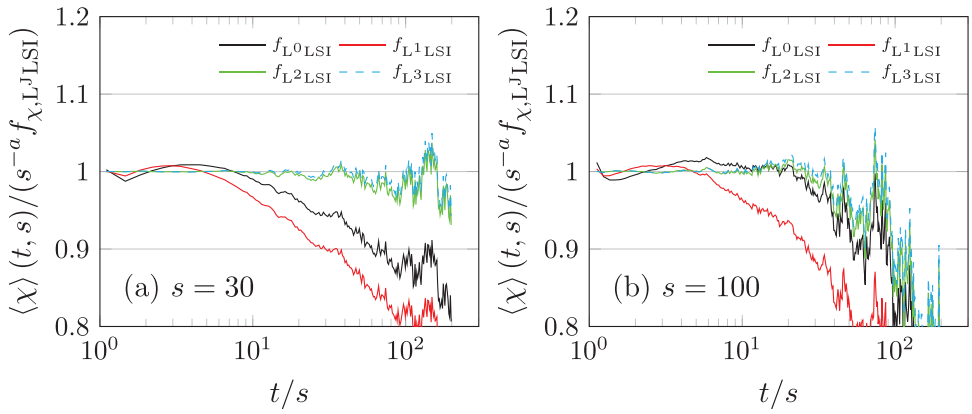

Figure 2. Plots of equation (15) in case of SCA autoresponse calculations with $p = 0.95$ and $q = 0$. Sample sizes are $n_{\mathrm{SCA},s=30} = 23\,849$ for $s = 30$ (a) and $n_{\mathrm{SCA},s=100} = 12012$ for $s = 100$ (b). Best fits are determined from the region $1 \leqslant t/s \leqslant 10$.

Table 2. Parameters for best fits of $f_{\chi,\mathrm{L^JLSI}}$ forms to KPZ autoresponse functions for $1 \leqslant t/s \leqslant 200$. Values for λ_R/z in parenthesis result from fits considering $q \leqslant t/s \leqslant 10$, as presented in figure 2. $a = 0.24$ for all fits. Error margins are not given, because the method employed for fitting does not provide meaningful estimates.

		λ_R/z	a'	A_0	A_1	A_2	A_3
$s = 30$	$f_{\mathrm{L^0LSI}}$	1.164 (1.167)	0.016	38.833			
	$f_{\mathrm{L^1LSI}}$	1.164 (1.144)	0.023	35.085	0.187		
	$f_{\mathrm{L^2LSI}}$	1.224 (1.219)	0.501	4.938	1.772	−0.431	
	$f_{\mathrm{L^3LSI}}$	1.224 (1.224)	0.505	4.790	1.716	−0.422	−0.004
$s = 100$	$f_{\mathrm{L^0LSI}}$	1.186 (1.191)	0.006	102.584			
	$f_{\mathrm{L^1LSI}}$	1.165 (1.142)	0.100	14.444	0.844		
	$f_{\mathrm{L^2LSI}}$	1.230 (1.224)	0.490	5.544	2.019	−0.472	
	$f_{\mathrm{L^3LSI}}$	1.230 (1.233)	0.475	5.506	1.914	−0.437	−0.008

$$\frac{\langle\chi\rangle(t/s)}{s^{-a}f_{\chi,\mathrm{L^JLSI}}(t/s)} \stackrel{!}{=} 1 \qquad \text{for } t/s > 1. \tag{15}$$

Non-linear fits for $J > 0$ do not converge using the classical least-squares Levenberg–Marquardt algorithm [45, 46]. To obtain the parameters presented in table 2, the Nelder–Mead method [47] was employed, which does not provide statistical error estimates for the fit parameters. Fit results can be governed by any of a multitude of local minima, depending on the initial guesses and the choosen fit interval. Judging by the connected variation in parameter values, the accuracy of the tabulated parameters should be assumed to be no better than 20%, except for the values of λ_R/z which vary by less than 5%.

It is apparent from figure 2 that the uncorrected LSI ansatz fails to describe the asymptotic behavior of χ, giving $\lambda_R/z \approx 1.17$. So does the logarithmic form with $J = 1$. The form with $J = 2$, which is predicted by the theory yields much better fits, with $\lambda_R/z \approx 1.22$, agreeing with the asymptotic value obtained earlier $\lambda_R^{\mathrm{tail}}/z = 1.23(2)$. The parameter fits presented in table 2 take into account the observed time interval $1 \leqslant t/s \leqslant 200$. When the fit is limited to the

interval $1 \leqslant t/s \leqslant 10$, the results for λ_R (values in parentheses) do not change significantly. This means, that the $f_{\chi,\mathrm{L^2LSI}}$ form describes the corrections, affecting the autoresponse function at early times, well enough to determine the correct asymptotic autoresponse exponent just using early-time data.

The form with $J = 3$ shows marginally better agreement with the data in figure 2. In fits to the whole observed time interval, the amplitude A_3 of the added third-order term is severely suppressed (table 2). Adding another fit parameter, a slightly better fit would be expected. The small absolute value of A_3 in relation to A_2 suggests, that a third order correction does not carry physical meaning, supporting the $\mathrm{L^2LSI}$ theory.

The values of the coefficients for $J = 2$ and 3 are similar at different waiting times. This satisfies our expectation, since aging is described by the s^{-a} term in equation (10) alone and the functional form of $f_\chi(t/s)$ should not depend on s explicitly. The autoresponse functions we obtained by less precise simulations also agree with the $\mathrm{L^2LSI}$ theory, but they exhibit too much noise to exclude a logarithmic series like (14).

In conclusion, we provide numerical evidence that the $\mathrm{L^2LSI}$ theory describes well aging data of the autoresponse function for all measured times in case of the $2 + 1$ dimensional KPZ surface growth. We obtained precise estimates for the autoresponse exponent as well as for the aging exponents. In particular a $\lambda_R = 2.00(6)$ estimate seems to emerge from our high precision parallel simulations. Our code can be extended to also calculate the space-dependent part of the KPZ response function. For the autocorrelation functions of the KPZ model $f_{C,\mathrm{L^2LSI}}$ a form is yet to be proposed. Our simulations generate high precision correlation data for heights as well as density variables that remains to be tested later against different aging functions [41].

Acknowledgments

We thank M Henkel for helpful discussions and comments. Support from the Hungarian research fund OTKA (Grant No. K109577), the Initiative and Networking Fund of the Helmholtz Association via the W2/W3 Program (W2/W3-026) and the International Helmholtz Research School NanoNet (VH-KO-606) is acknowledged. We gratefully acknowledge computational resources provided by the HZDR computing center, NIIF Hungary and the Center for Information Services and High Performance Computing (ZIH) at TU Dresden.

References

[1] Ódor G 2008 *Universality in Nonequilibrium Lattice Systems* (Singapore: World Scientific)
[2] Täuber U C 2014 *Critical Dynamics* (Cambridge: Cambridge University Press)
[3] Struik L C E 1978 *Physical Aging in Amorphous Polymers and Other Materials* (Amsterdam: Elsevier)
[4] Henkel M 1994 *J. Stat. Phys.* **75** 1023–61
[5] Cardy J L 1996 *Scaling and Renormalization in Statistical Mechanics* (Cambridge: Cambridge University Press)
[6] Henkel M 1999 *Conformal Invariance and Critical Phenomena* (Berlin: Springer)
[7] Henkel M and Pleimling M 2010 *Non-Equilibrium Phase Transitions: Ageing and Dynamical Scaling Far from Equilibrium* (*Theoretical and Mathematical Physics* vol 2) (New York: Springer)
[8] Hinrichsen H 2008 *J. Stat. Mech.* P07026
[9] Gurarie V 1993 *Nucl. Phys.* B **410** 535–49
[10] Henkel M 2013 *Nucl. Phys.* B **869** 282–302

[11] Hohenberg P C and Halperin B I 1977 *Rev. Mod. Phys.* **49** 435–79
[12] Bray A 1994 *Adv. Phys.* **43** 357–459
[13] Cugliandolo L F 2003 *Les Houches—Ecole d'Ete de Physique Theorique* vol 77 (Berlin: Springer)
[14] Henkel M and Durang X 2015 *J. Stat. Mech.* P05022
[15] Henkel M 2015 *Symmetry* **7** 2108
[16] Edwards S F and Wilkinson D R 1982 *Proc. R. Soc.* A **381** 17–31
[17] Henkel M 2017 *Symmetry* **9** 2
[18] Enss T, Henkel M, Picone A and Schollwöck U 2004 *J. Phys. A: Math. Gen.* **37** 10479
[19] Ódor G 2006 *J. Stat. Mech.* L11002
[20] Henkel M 2007 *J. J. Phys.: Condens. Matter.* **19** 065101
[21] Hinrichsen H 2006 *J. Stat. Mech.* L06001
[22] Henkel M, Noh J D and Pleimling M 2012 *Phys. Rev.* E **85** 030102
[23] Ódor G, Liedke B and Heinig K H 2009 *Phys. Rev.* E **79** 021125
[24] Kelling J and Ódor G 2011 *Phys. Rev.* E **84** 061150
[25] Ódor G, Kelling J and Gemming S 2014 *Phys. Rev.* E **89** 032146
[26] Kardar M, Parisi G and Zhang Y C 1986 *Phys. Rev. Lett.* **56** 889–92
[27] Burgers J M 1974 *The Nonlinear Diffusion Equation: Asymptotic Solutions and Statistical Problems* (Boston, MA: D Reidel Pub. Co) (first published in 1973 under title: Statistical problems connected with asymptotic solutions of the one-dimensional nonlinear diffusion equation)
[28] Halpin-Healy T 1990 *Phys. Rev.* A **42** 711–22
[29] Forster D, Nelson D R and Stephen M J 1977 *Phys. Rev.* A **16** 732–49
[30] Kardar M 1985 *Phys. Rev. Lett.* **55** 2923–3
[31] van Beijeren H, Kutner R and Spohn H 1985 *Phys. Rev. Lett.* **54** 2026–9
[32] Janssen H and Schmittmann B 1986 *Z. Phys.* B **63** 517–20
[33] Hwa T 1992 *Phys. Rev. Lett.* **69** 1552–5
[34] Family F and Vicsek T 1985 *J. Phys. A: Math. Gen.* **18** L75
[35] Meakin P, Ramanlal P, Sander L M and Ball R C 1986 *Phys. Rev.* A **34** 5091–103
[36] Barabási A and Stanley H 1995 *Fractal Concepts in Surface Growth* (Cambridge: Cambridge University Press) (https://books.google.de/books?id=W4SqcNr8PLYC)
[37] Krug J 1997 *Adv. Phys.* **46** 139–282
[38] Halpin-Healy T and Palasantzas G 2014 *Europhys. Lett.* **105** 50001
[39] Carrasco I S S, Takeuchi K A, Ferreira S C and Oliveira T J 2014 *New J. Phys.* **16** 123057
[40] Kelling J, Ódor G, Nagy M F, Schulz H and Heinig K 2012 *Eur. Phys. J. Spec. Top.* **210** 175–87
[41] Kelling J, Ódor G and Gemming S 2017 to be published
[42] Kelling J, Ódor G and Gemming S 2016 Bit-vectorized GPU implementation of a stochastic cellular automaton model for surface growth *IEEE Int. Conf. on Intelligent Engineering Systems* (IEEE) (doi: 10.1109/INES.2016.7555127)
[43] Kallabis H and Krug J 1999 *Europhys. Lett.* **45** 20
[44] Krech M 1997 *Phys. Rev.* E **55** 668–79
[45] Levenberg K 1944 *Q. J. Appl. Math.* **II** 164–8
[46] Marquardt D W 1963 *J. Soc. Ind. Appl. Math.* **11** 431–41
[47] Nelder J A and Mead R 1965 *Comput. J.* **7** 308–13